*Acta of Bioengineering and Biomechanics*
*Vol. 15, No. 1, 2013*

Original paper
DOI: 10.5277/abb130106

# Numerical investigation of root canal irrigation adopting innovative needles with dimple and protrusion

PING LI, DI ZHANG*, YONGHUI XIE, JIBING LAN

Key Laboratory of Thermal Fluid Science and Engineering of Ministry of Education,
School of Energy and Power Engineering, Xi'an Jiaotong University, Xi'an, P.R. China.

As important passive flow control methods, dimples and protrusions have been successfully implemented via geometric modifications to manipulate flow fields to get a desired flow parameters enhancement. In this research, two novel needles were proposed based on a prototype by means of the dimple and protrusion, and flow patterns within a root canal during final irrigation with these needles were numerically investigated. The calculation cases consistent with the clinically realistic irrigant flow rates, which are 0.02, 0.16 and 0.26 mL $s^{-1}$ are marked as case A, B and C, respectively. The characteristic parameters to estimate irrigation efficiency, such as shearing effect, mean apical pressure, irrigation replacement and fluid agitation, were compared and the optimal geometry in every calculation case was obtained. As shown from the results, flow rates and needle geometries were the causes of irrigation parameters variations. The sum of shear stress, irrigation replacement and fluid agitation were equal in the low flow rate case A, however, the needle with a protrusion on its tip had advantages in the three irrigation characteristic parameters above in calculation case B, and the needle with a dimple on its tip had advantages in calculation case C. Furthermore, the needles proposed did not give rise to the risk of irrigant extrusion. These needles can be better choices at larger flow rates. Therefore, needle geometry optimizations utilizing passive flow control methods are worthy to be investigated in the root canal irrigation enhancement.

*Key words*: *dimple, protrusion, innovative needles, numerical simulation, passive flow control methods, root canal irrigation*

## 1. Introduction

Root canal irrigation is a fundamental procedure to facilitate removal of bacteria, debris, biofilm and therapeutic materials by means of irrigant fluid mechanical action, especially from the areas that have not been prepared completely by mechanical instruments [1], [2]. It has been shown that 35% or more of the root canal system is untouched by endodontic instruments because of its complexity, which highlights the importance of root canal irrigation in canal preparation process [3]. The chemical ability of irrigant is mainly to kill bacteria and dissolve organic and inorganic tissue in the direct contact area, whereas fluid mechanical action has more effect on mixture of irrigant within the canal lumen and removal of adhesive biofilm and smear layer on the canal wall. The detailed flow structures and parameters in the flow field are the reflection of flow mechanical action, so evaluating the irrigation efficacy of debridement and irrigant replacement could be accomplished by analyzing irrigant flow dynamics.

Computational fluid dynamics (CFD) is a valuable research tool for investigating flow patterns by mathematical modeling and computer simulation. Although CFD was widely used in industrial and engineering applications [4]–[6], recent research shows that utilizing CFD in biomechanics reasonable results are obtained, especially in conditions in which in vivo and ex vivo experiments are hard to carry out due to the limited testing means or expenses [7]–[11]. Re-

* Corresponding author: Di Zhang, Key Laboratory of Thermal Fluid Science and Engineering of Ministry of Education, School of Energy and Power Engineering, Xi'an Jiaotong University, Xi'an, Shaanxi Province, 710049, P.R. China. Tel: 86-29-8266-4443(O), fax: 86-29-8266-4443, e-mail: zhang_di@mail.xjtu.edu.cn

Received: March 19th, 2012
Accepted for publication: November 25th, 2012

cently, based on many CFD investigations, irrigant flow patterns in the root canal lumen have been obtained [12]–[15]. The results above show that the geometry of needle affects the irrigant replacement effectiveness significantly, so the focus of this research is to investigate the influence of needle geometry innovation on irrigation efficiency.

The ability to manipulate a flow field to effect a desired change is of immense practical importance, so flow control is perhaps more hotly pursued by scientists and engineers than any other area in fluid mechanics [16]. As an important aspect, passive flow control has been successfully implemented via geometric modifications. Dimples and protrusion devices are so adaptive to various operating conditions and easy to manufacture that they are always selected as a passive flow control method. Utilizing these devices, the desired effects, such as enhancement of fluid mixture and diversiform fluid characteristics, are obtained [17]–[20]. The authors also investigated the effects of dimple and protrusion on the flow structures and heat transfer enhancement resulting from fluid mixture, and optimized the dimple and protrusion constructions and combinations [21], [22].

Based on the previous studies on the flow control, the advantages of enhancing fluid mixture of the dimple and protrusion were obtained, however, little research has been conducted on the effect of the flow control method on the irrigation efficiency, so two novel needles with dimple and protrusion were proposed based on a prototype in the present study. Furthermore, in search for the optimal needle geometry for irrigation using various flow rates, based on an experimental validated CFD model, flow patterns within the prepared root canal during final irrigation with these needles were investigated. The characteristic parameters to estimate irrigation efficiency, such as shearing effect, mean apical pressure and irrigation replacement and fluid agitation [23], were compared among three needles and the optimal geometry in special calculation case was obtained.

# 2. Materials and methods

## 2.1. Geometry

Similar to a previous study [24], 30G KerrHawe Irrigation Probe needle was selected as the prototype (named needle I) in this study, where $D_{ext}$ = 320 μm, $D_{int}$ = 196 μm, $l$ = 31 mm represented the external and internal diameter and the length of needle I, respectively. Based on needle I, two novel needles with passive flow control device were proposed. There was a protrusion with a height of 0.03 mm and a diameter of 0.09 mm on the tip of needle II; moreover, there was a dimple with a depth of 0.04 mm and diameter of 0.17 mm on the top of needle III. The other features of needles II and III were the same as those of needle I. Detailed geometries are shown in Fig. 1.

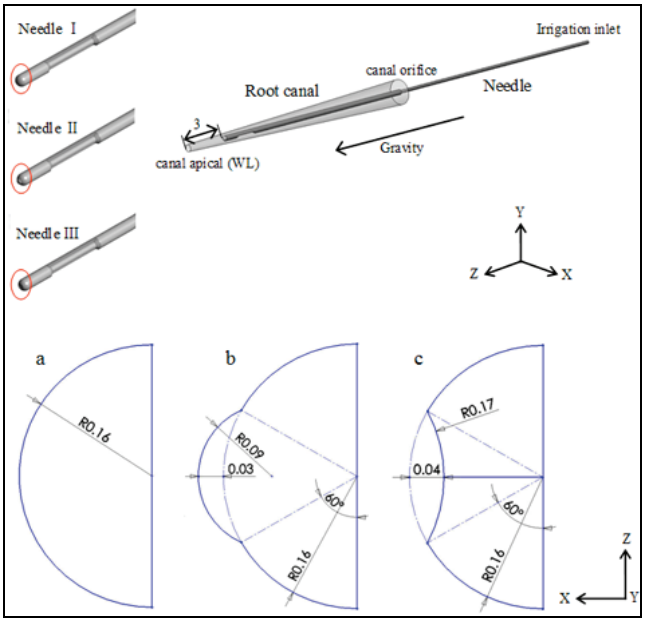


Fig. 1. Geometry structure of irrigation system and detailed characteristics of needle prototype and variations, where the tips of needles I, II, III are marked with red eclipse, and enlarged drawings on X-Z plane are shown in figures a, b and c, respectively (unit: mm)

The root canal was simulated as a geometrical frustum of a cone of 18 mm in length, with a diameter of 0.45 mm at the apical surface and a diameter of 1.57 mm at the canal orifice surface (6.2% taper). The needle was fixed and centred within the canal, 3 mm short of the canal apical surface (Fig. 1), which was a reasonable way to judge the effect of irrigant flowing to the space between the needle tip and the canal apical surface.

## 2.2. Grid generation

For the purpose of increasing the accuracy and validity of the model, an all-hexahedral mesh was generated and refined near the walls and in the areas where high gradients of variables were anticipated. To enhance the quality of meshes in the flow channel, the region near curvature surfaces, such as the near-wall

regions and flow control devices, were O-type meshed, meanwhile, the far-wall region was H-type meshed (see Fig. 2). Balancing the simulation accuracy and computational resource, a grid-independence check was carried out to determine reasonable grid nodes for computational analysis (Table 1), where the mean apical pressure was chosen as the evaluation criterion. As is shown, the relative discrepancy was just 0.054% adopting 2.12 million computational nodes, therefore, the proposed mesh was the calculation condition 4, whose minimum orthogonality angle was 35 degree and maximum mesh expansion factor was 9.9.

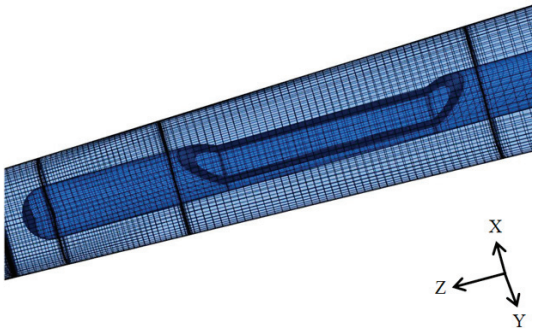


Fig. 2. Computational mesh of key region

Table 1. Verification of grid independence in computational domain

| Calculation conditions | Number of nodes/million | Mean apical pressure/kPa | Relative discrepancy (%) |
|---|---|---|---|
| 1 | 1.2 | 10.221 | — |
| 2 | 1.86 | 10.168 | 0.52 |
| 3 | 2.03 | 10.156 | 0.12 |
| 4 | 2.12 | 10.150 | 0.054 |

## 2.3. Boundary conditions and solver setup

To simulate the clinical irrigation conditions, the walls of the canal and the needle were set as impermeable and no-slip boundary conditions, irrigation inlet as shown in Fig. 1, and canal orifice was set as outlet. As is shown in Table 2, consistent with the clinically realistic irrigant flow rates [25], constant axial velocities were imposed at the inlet for all the cases studied, normal to the surface. A pressure outlet boundary condition was set at the outlet surface, whose value was that of atmospheric pressure. Gravity was included in the flow field in the direction of positive $z$-axis and the turbulence model was none [24]. Sodium hypochlorite 1% aqueous solution [26] with density $\rho$ equal to 1040 kg m$^{-3}$ and viscosity $\mu$ equal to 0.986 10$^{-3}$ Pa s was selected as the irrigant.

Table 2. Inlet boundary condition for the cases studied

| Calculation cases | Irrigant flow rate (mL s$^{-1}$) | Reynolds number at the needle inlet | Inlet velocity (m s$^{-1}$) |
|---|---|---|---|
| A | 0.02 | 137 | 0.7 |
| B | 0.16 | 1096 | 5.3 |
| C | 0.26 | 1678 | 8.6 |

The equations for conservation of mass (continuity equation) and conservation of momentum in an inertial (non-accelerating) reference frame can be written as follows

$$\frac{\partial \rho}{\partial t} + \nabla \cdot (\rho \vec{v}) = 0, \tag{1}$$

$$\frac{\partial}{\partial t}(\rho \vec{v}) + \nabla \cdot (\rho \vec{v} \vec{v}) = -\nabla p + \rho \vec{g}, \tag{2}$$

where $p$ is the static pressure, $\vec{v}$ is the fluid velocity vector, and $\rho \vec{g}$ is the gravitational body force. The above equations were solved by an implicit solver adopting a finite volume approach to analyze this problem. An unsteady simulation was carried out without turbulence model in the study as the Reynolds numbers were so small that laminar flow was anticipated. The time-step was set at 10$^{-6}$ s and total time was 50 ms for the real flow time. The convergence criterion was 10$^{-5}$ to ensure more reasonable results. The numerical calculations were conducted by means of a commercial CFD code FLUENT6.3. The hardware of the computational system consists of four Intel Xeon CPUs at 2.8 GHz, an internal memory with capacity of 32 G and a hard disk with capacity of 1 T. The start method of the parallel environment is mpich2 local parallel for Windows. The time for each calculation case is about 14 hours.

## 2.4. Validation of the CFD model

Calculation condition C was chosen to validate the CFD model and compare with the PIV experiment results [24]. The PIV images were recorded at a speed of up to 250 000 frames s$^{-1}$ and the exposure time was set to one-eight of the inter-frame time. The computational process adopted in this study was completely consistent with that proposed by Boutsioukis et al. For explanatory purposes, the flow velocity contours and vectors of the most critical region in the Z-Y plane and Z-X plane were illustrated in order to compare them with PIV results (Fig. 3). As was shown, the CFD results were in good agreement with PIV results in terms of fluid velocity distributions and directions

at the needle ejection region and the main action extent. The tiny distinction shown was possibly due to the inherent limitation of the test method, mainly in the vicinity of canal wall. Velocity was calculated in an interrogation area in the PIV code, instead of a single point, moreover, in the vicinity of canal wall, the interrogation area is comprised of the fluid region and the wall, so the average of this area may lead to velocity deviation. The tiny distinction is usually accepted in the simulation model validation [24]. Therefore, the CFD model proposed in this study was reasonable to simulate needle irrigation process generally.

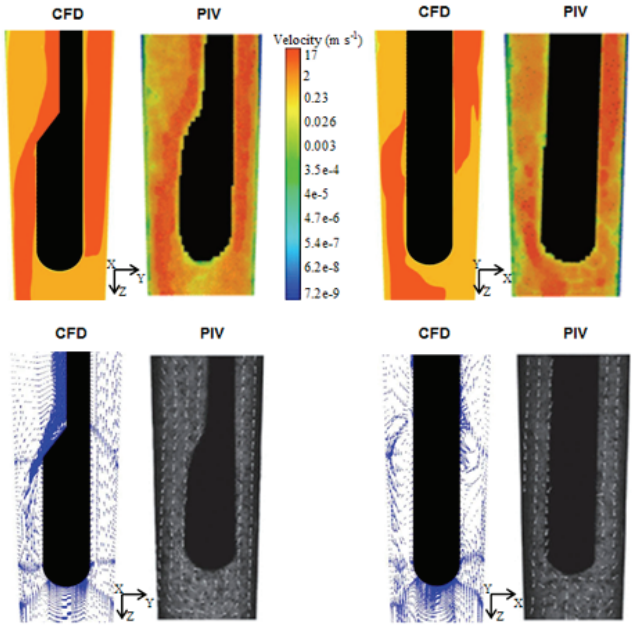


Fig. 3. Velocity contours and vectors along the Z-Y (side view) and Z-X (front view) plane of the key region. PIV results close to the wall of the root canal are not considered accurate due to inherent limitation of PIV method [24]

# 3. Results

The fluid field results revealed that the irrigant flow fully developed in the needle lumen before reaching the needle outlet, then it formed a side impinging jet in the vicinity of the needle outlet because of the sudden expansion of the flow region, next the jet flowed to the tip of the needle and twisted around there motivated by some Moffatt's corner vortices, finally the irrigant flowed to the canal outlet mainly from the channel behind the needle outlet. During the irrigating process, bacteria, debris, biofilm and therapeutic materials within the canal and on the canal wall were taken away by the irrigant flushing effect.

## 3.1. Analysis of irrigation increasing depth and irrigant agitation

An important role of root canal irrigation was to remove the debris and enhance irrigant exchange. Within canal, velocities higher than 0.1 m $s^{-1}$ were considered clinically significant for adequate irrigant replacement. Therefore, time averaged distributions of the axial Z-component of irrigant velocity near the needle tip were extracted to analyze irrigant replacement potency (see Fig. 4), and increasing depth, defined as the farthest place distal to the needle tip where velocity was higher than 0.1 m $s^{-1}$, was compared among three needles (see Table 3). Time averaged stream-lines of apical third in calculation case C demonstrated fluid dynamics near the needle tip, the needle tip geometrical feature affected the flow condition to a large extent, and needle III was far superior to others in terms of increasing depth and irrigant agitation. Furthermore, velocity distributions also verified this; in detail, velocity distributions near the

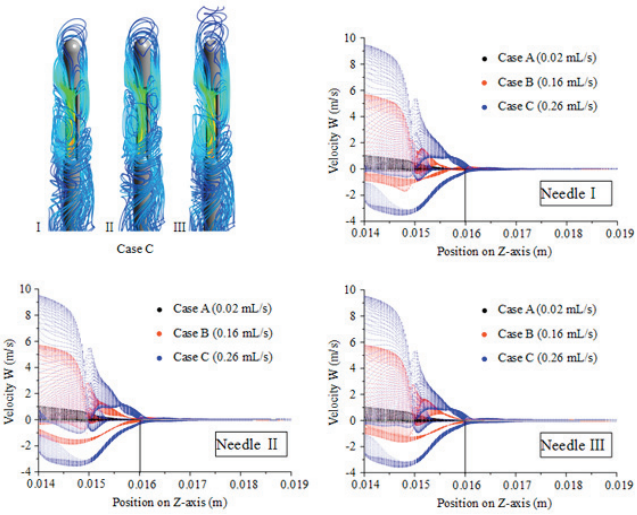


Fig. 4. Stream-lines provide visualization of irrigant flow path, using some mass-less particles released from needle inlet. Time averaged velocity W (Z-component) of irrigant along *Z*-axis for all the cases and all the needle geometries studied, which reflect the increasing depth of irrigant replacement and velocity fluctuation near needle tip. In *Z*-axis, 0.016 m (labeled as black line) is the position of needle tip, and 0.019 m is the canal orifice plane

Table 3. Time averaged increasing depth of irrigant replacement (mm)

| Calculation cases | Needle I (prototype) | Needle II | Needle III |
|---|---|---|---|
| A | 0.15 | 0.15 | 0.15 |
| B | 0.52 | 0.69 | 0.63 |
| C | 0.84 | 1.08 | 1.27 |

needle tip were basically the same in case A, whereas in cases B and C, velocity fluctuated more intensely using needles II and III, especially in the range of 0.015–0.016 m, and penetrated much further than needle I. The statistical data listed in Table 3 shed light on the increasing depth difference among the three needles. Irrigant penetrations were equal at low flow rate, as flow rate increased, the differences became gradually distinct, and the needles with dimple and protrusion had an advantage over the prototype in view of increasing depth. When the flow rate was 0.16 mL/s, the increasing depth of needle I was 0.52 mm, whereas it was 0.69 mm and 0.63 mm for needles II and III, respectively. For the flow rate of 0.62 mL/s, needles II and III had the potential to achieve increasing depth as far as 1.08 mm and 1.27 mm, much further than 0.84 mm, which was the prototype irrigation increasing depth.

## 3.2. Analysis of wall shear stress

Irrigation effect relied partly on the irrigant flushing within the root canal, and partly on the irrigant dissolution and physical shearing on the canal wall generated by fluid flow, where the latter was the key cause for biofilm and smear layer removal. Therefore, shear stresses on the canal wall should be analyzed to find a better choice. Time averaged sums of shear stress on canal wall of all the needles (WSS, for short) studied for different calculation cases are compared in Fig. 5. The results showed that WSS primarily depended on flow rates. As flow rate increased, WSS increased gradually. Furthermore, geometrical features of the needle tip affected WSS simultaneously. For calculation case A, WSS of all the needles were equal to each other. In case B, the largest and smallest values of the sum of stress were obtained by employing needles II and I, respectively. In case C, the smallest value was also generated by needle I, however, the largest value was produced by needle III. In case B, the differences among the three needles were smaller, but in case C, the differences were comparatively large. As a result, needles II and III were better than needle I in respect of the needle wall shearing effect at a large flow rate.

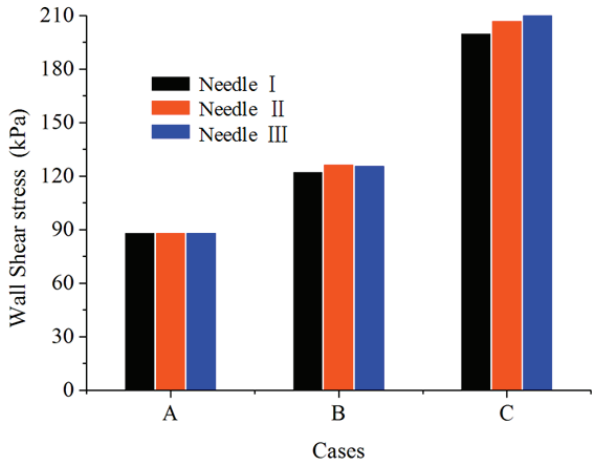


Fig. 5. Time averaged sums of wall shear strain rate (WSS) of all the cases and all the geometries studied, indicating the irrigant shearing effect on the root canal wall. The irrigant dissolving and removal potency on the root canal wall was obtained

## 3.3. Analysis of mean apical pressure

Under the root canal irrigation procedure, irrigant extrusion occurred as a diffusion of the spent irrigant into the periapical tissues, and adverse reactions, such as tissue irritation, may be caused by adopting sodium hypochlorite as irrigant, so that a sufficient volume is extruded. Therefore, mean apical pressure of root canal should be analyzed to estimate the risk of irrigant extrusion and to evaluate the whole performance of irrigation [23]. Time averaged mean apical pressures of all the needles studied for different calculation cases are shown in Fig. 6. The results showed that the mean apical pressure primarily depended on flow rates. As the flow rate increased, especially from cases B to C, mean apical pressure increased gradually, however, mean apical pressures for all the needles were almost equal in the same calculation case. In calculation case A, mean apical pressures of all the needles were equal to each other. In case B, there were minor differences among the three needles,

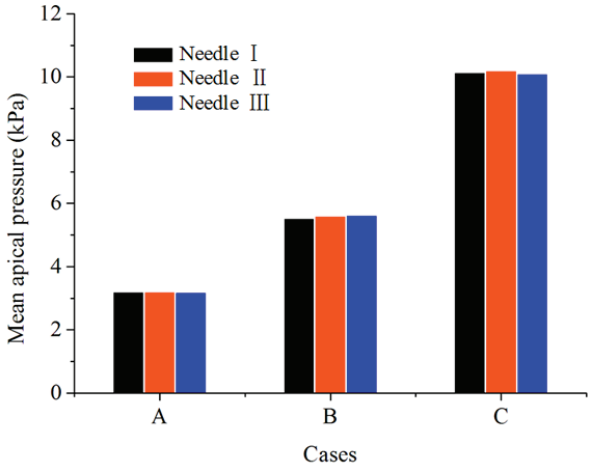


Fig. 6. Time averaged mean pressure at the root canal apical plane of all the cases and all the needles studied, implying the risk of extrusion to periapical tissues

and the largest and smallest values were produced by needles III and I, respectively. In case C, mean apical pressure adopting needle II was larger than others, and needle I produced the smallest value while irrigating.

# 4. Discussion

Generally, the numerical simulation model proposed should be validated by related experimental results. For CFD models, the flow field visualization technique PIV is usually selected as the validation method. In the present study, the simulated flow velocity contours and vectors were compared with PIV results (Fig. 3). As was shown, CFD results were in good agreement with PIV results, except the tiny distinction mainly in the vicinity of canal wall, which is possibly due to the inherent limitation of test method. The velocity was calculated in a interrogation area in the PIV code, instead of a single point, moreover, in the vicinity of canal wall, the interrogation area is comprised of the fluid region and the wall, so the average of this area may lead to the deviation of velocity. A tiny distinction is usually accepted in the simulation model validation [24]. Therefore, the CFD model proposed in this study was reasonable to simulate needle irrigation process generally.

The needles proposed had advantages in irrigant penetration, especially at higher flow rate, which made it possible to enhance the fluid mixing and exchange at the top of the canal, so the irrigation efficiency could be improved. Adopting needles II and III, more violent flow velocity fluctuation emerged in the range from the needle outlet to its tip in cases B and C, which induced stronger impact and disinfection on the canal wall and also was a potential power to penetrate further. As a result, in respect of irrigant penetration and fluid agitation, the needles proposed, needle II for case B and needle III for case C, might be a better choice. Although the absolute values improved of increasing depth were small, the values relative to that of prototype were very large, so it was meaningful to use these flow control devices. Utilizing the dimple and protrusion to improve irrigation efficiency was a beneficial attempt; in addition, associated with geometrical construction optimization of dimple and protrusion one could obtain some other better results.

Combining the flow field velocity analysis, the reason why WSS differed among the three needles might be that as the flow rate rose, the flow within the root canal was more turbulent adopting novel needles (Fig. 4), so the interaction between irrigant flow and root canal wall advanced, in addition, the penetration and increasing depth for irrigant replacement were further using needles II and III (Table 3), resulting in more extended flushing region, consequently, WSS rose due to the joint action of these two aspects.

In our research, WSS was used to analyze irrigant flow shearing effect, instead of the contour of shear stress distribution, which was because: 1) although the shearing effect on the canal wall was improved employing needles with dimple and protrusion, a relatively small difference could not yet be reflected clearly in shear stress contours, while the bar chart could show it intuitively; 2) the key region studied was the apical third of root canal, and the main differences also emerged here, whereas other region was basically identical, so the difference of WSS could reflect the shear stress difference on the apical third canal wall; moreover, the whole shearing effect not only acted on the apical third region, but also the other region, so WSS could be regarded as the integrated difference of the shearing effect, which was more informative.

Summarizing the above results of the analysis, a noteworthy finding of this study was the advantages of the proposed needles with dimple and protrusion while irrigating. As shown from the results, the proposed needles had advantages in increasing depth of irrigant flushing, fluid agitation (Fig. 4 and Table 3) and canal wall shearing effect (Fig. 5). Moreover, another heartening finding was the minor difference of mean apical pressure while irrigating employing the needles proposed (Fig. 6), which meant that utilizing these needles, the irrigating shearing effect on the root canal wall and flushing effect within the root canal lumen advanced, meanwhile, the risk of extrusion did not increase, so the whole performance of root canal irrigation was reasonably improved. The results verified that the passive control devices, dimple and protrusion, were useful to control the flow field inside root canal lumen to improve irrigating effect, and some further research should be worth conducting, such as optimization of the geometry, number and position of dimple and protrusion to produce higher irrigation efficiency.

Micro-Electro-Mechanical System (MEMS) is a booming micro-fabrication technology, and is used widely in healthcare and medical devices [27]. Although the dimple and protrusion devices on the tip of the needles proposed are small, they can yet be fabricated precisely by means of MEMS technology, and optimization of flow control devices can also be conducted easily.

# 5. Conclusions

The irrigation flow fields within a prepared root canal employing three needles with different tip geometrical feature at different flow rates were investigated, and the whole irrigation performances were compared to find a better choice for the specific condition. The main conclusions are as follows:

1) Flow rates are the dominant causes of the changes of irrigation replacement, fluid agitation, shear stress on the canal wall and mean apical pressure within fluid domain, however, the differences due to the changes of the needle tip geometry are also significant in some calculation cases.

2) Irrigation replacement, fluid agitation and shearing effect are equal at low flow rate, whereas, the needles with passive control devices are more useful for fluid mixture, biofilm and smear layer removal at larger flow rates.

3) Mean apical pressures for the three needles are almost equal in the same calculation case, except minor differences, which means that the needles with passive control devices have not given rise to the risk of irrigant extrusion.

In summary, flow control methods, as a powerful method for obtaining favored flow change, can also be used to enhance root canal irrigation effect. The present study is a beneficial exploration to discover the significance of flow control methods on root canal irrigation, and the results clarify the orientation to endeavor. Investigation on the effects of geometry, number and position of dimple and protrusion devices on the irrigation efficiency may be a promising research direction.

## Acknowledgements

This work was supported by the Fundamental Research Funds for the Central Universities (Grant No. XJJ20100127).

## References

[1] LEE S.J., WU M.K., WESSELINK P.R., *The effectiveness of syringe irrigation and ultrasonics to remove debris from simulated irregularities within prepared root canal walls*, International Endodontic Journal, 2004, 37(10), 672–678.

[2] GULABIVALA K., PATEL B., EVANS G., NG Y.L., *Effects of mechanical and chemical procedures on root canal surfaces*, Endodontic Topics, 2005, 10(1), 103–122.

[3] PETERS O.A., SCHÖNENBERGER K., LAIB A., *Effects of four Ni–Ti preparation techniques on root canal geometry assessed by micro computed tomography*, International Endodontic Journal, 2001, 34(3), 221–230.

[4] LÓPEZ P.A., MORA J.J., MARTÍNEZ F.J., IZQUIERDO J., *Computational fluid dynamics (CFD) models in the learning process of Hydraulic Engineering*, Computer Applications in Engineering Education, 2010, 18(2), 252–260.

[5] MOULLEC Y. LE, GENTRIC C., POTIER O., LECLERCA J.P., *CFD simulation of the hydrodynamics and reactions in an activated sludge channel reactor of wastewater treatment*, Chemical Engineering Science, 2010, 65(1), 492–498.

[6] XIA H., TUCKER P.G., DAWES W.N., *Level sets for CFD in aerospace engineering*, Progress in Aerospace Sciences, 2010, 46(7), 274–283.

[7] STEINMAN D.A., VORP D.A., ETHIER C.R., *Computational modeling of arterial biomechanics: Insights into pathogenesis and treatment of vascular disease*, Journal of Vascular Surgery, 2003, 37(5), 1118–1128.

[8] LUO H.Y., LIU Y., *Modeling the bifurcating flow in a CT-scanned human lung airway*, Journal of Biomechanics, 2008, 41(12), 2681–2688.

[9] AI L.S., YU H.Y., TAKABE W., PARABOSCHI A., YU F., KIM E.S., Li R.S., HSIAI T.K., *Optimization of intravascular shear stress assessment in vivo*, Journal of Biomechanics, 2009, 42(10), 1429–1437.

[10] DI Y.J., FEI M.R., SUN X., YANG T.C., *Modeling of the Human Bronchial Tree and Simulation of Internal Airflow: A Review*, Life System Modeling and Intelligent Computing, 2010, 6328, 456–465.

[11] LOVALD S., HEINRICH J., KHRAISHI T., YONAS H., PAPPU S., *The role of fluid dynamics in plaque excavation and rupture in the human carotid bifurcation: a computational study*, International Journal of Experimental and Computational Biomechanics, 2009, 1(1), 76–95.

[12] BOUTSIOUKIS C., LAMBRIANIDIS T., KASTRINAKIS E., BEKIAROGLOU P., *Measurement of pressure and flow rates during irrigation of a root canal ex vivo with three endodontic needles*, International Endodontic Journal, 2007, 40(7), 504–513.

[13] BOUTSIOUKIS C., VERHAAGEN B., VERSLUIS M., KASTRINAKIS E., WESSELINK P.R., SLUIS L.W.M., *Evaluation of irrigant flow in the root canal using different needle types by an unsteady computational fluid dynamics model*, Journal of Endodontics, 2010, 36(5), 875–879.

[14] GAO Y., HAAPASALO M., SHEN Y., WU H.K., LI B.D., RUSE N.D., ZHOU X.D., *Development and validation of a three-dimensional Computational Fluid Dynamics model of root canal irrigation*, Journal of Endodontics, 2009, 35(9), 1282–1287.

[15] SHEN Y., GAO Y., QIAN W., RUSE N.D., ZHOU X.D., WU H.K., HAAPASALO M., *Three-dimensional numeric simulation of root canal irrigant flow with different irrigation needles*, Journal of Endodontics, 2010, 36(5), 884–889.

[16] GAD-EL-HAK M., *Modern developments in flow control*, Applied Mechanics Reviews, 1996, 49, 365–379.

[17] BEARMAN P.W., HARVEY J.K., *Control of circular cylinder flow by the use of dimples*, AIAA Journal, 1993, 31(10), 1753–1756.

[18] LIGRANI P.M., HARRISON J.L., MAHMMOD G.I., HILL M.L., *Flow structure due to dimple depressions on a channel surface*, Physics of Fluids, 2001, 13(11), 3442–3451.

[19] SYRED N., KHALATOV A., KOZLOV A., SHCHUKIN A., AGACHEV R., *Effect of surface curvature on heat transfer and hydrodynamics within a single hemispherical dimple*, Journal of Turbomachinery, 2001, 123(3), 609–613.

[20] PARK J., LIGRANI P.M., *Numerical predictions of heat transfer and fluid flow characteristics for seven different dimpled*

*surfaces in a channel*, Numerical Heat Transfer, Part A: Applications, 2005, 47(3), 209–232.

[21] LAN J.B., XIE Y.H., ZHANG D., *Effect of leading edge boundary layer thickness on dimple flow structure and separation control*, Journal of Mechanical Science and Technology, 2011, 25(12), 3243–3251

[22] LAN J.B., XIE Y.H., ZHANG D., *Flow and Heat Transfer in Microchannels with Dimples and Protrusions*, Journal of Heat transfer, 2012, 134(2), 021901-1-9.

[23] GULABIVALA K., NG Y.-L., GILBERTSON M., EAMES I., *The fluid mechanics of root canal irrigation*, Physiological Measurement, 2010, 31, R49–R84.

[24] BOUTSIOUKIS C., VERHAAGEN B., VERSLUIS M., KASTRINAKIS E., SLUIS L.W.M., *Irrigant flow in the root canal: experimental validation of an unsteady Computational Fluid Dynamics model using high-speed imaging*, International Endodontic Journal, 2010, 43(5), 393–403.

[25] BOUTSIOUKIS C., LAMBRIANIDIS T., KASTRINAKIS E., *Irrigant flow within a prepared root canal using various flow rates: a Computational Fluid Dynamics study*, International Endodontic Journal, 2009, 42(2), 144–155.

[26] CLEGG M.S., VERTUCCI F.J., WALKER C., BELANGER M., BRITTO L.R., *The effect of exposure to irrigant solutions on apical dentin biofilms in vitro*, Journal of Endodontics, 2006, 32(5), 434–437.

[27] PIMPIN A., SRITURAVANICH W., *Review on micro- and nanolithography techniques and their applications*, Engineering Journal, 2012, 16(1), 37–55.